

# Engineering Domain-Wall Motion in Co-Fe-B/MgO Ultrathin Films with Perpendicular Anisotropy Using Patterned Substrates with Subnanometer Step Modulation

A. Digiacoimo,<sup>1,2,3</sup> R. Mantovan,<sup>1,\*</sup> N. Vernier,<sup>3</sup> T. Devolder,<sup>3</sup> K. Garcia,<sup>3</sup> G. Tallarida,<sup>1</sup> M. Fanciulli,<sup>1,2</sup>  
A. Lamperti,<sup>1</sup> B. Ocker,<sup>4</sup> L. Baldi,<sup>5</sup> M. Mariani,<sup>5</sup> and D. Ravelosona<sup>3,†</sup>


<sup>1</sup>*CNR-IMM Unit of Agrate Brianza, Via C. Olivetti 2, 20864 Agrate Brianza, MB, Italy*

<sup>2</sup>*Department of Materials Science, University of Milano-Bicocca, Milano, Italy*

<sup>3</sup>*Center for Nanoscience and Nanotechnology (C2N), Université Paris Sud-CNRS, 91120 Palaiseau, France*

<sup>4</sup>*Singulus Technology AG, Hanauer Landstrasse 103, 63796 Kahl am Main, Germany*

<sup>5</sup>*Micron Semiconductor Italia S.r.l., Via Torri Bianche 24, Vimercate, MB 20871, Italy*

 (Received 13 December 2017; revised manuscript received 23 July 2018; published 21 December 2018)

Control of magnetic domain-wall motion in nanowires has attracted great interest due to the possibility to develop nonvolatile memory and logic circuits. We show that efficient domain-wall pinning can be engineered by growing Co-Fe-B/MgO ultra-thin magnetic films with perpendicular anisotropy on a patterned substrate exhibiting subnanometer steps modulation. The ratio of domain-wall velocity along and across the steps is found to be as high as 70, which corresponds to a variation of the depinning field up to 7 mT demonstrating a very efficient storing pinning scheme. In addition, we demonstrate very efficient domain-wall motion along the 70 nm conducts separating the steps. Our approach is compatible with nanoscale devices and large-scale mass production, opening new opportunities for domain-wall storage applications.

DOI: [10.1103/PhysRevApplied.10.064053](https://doi.org/10.1103/PhysRevApplied.10.064053)

## I. INTRODUCTION

The recent discovery that magnetic domain walls (DWs) can be moved under polarized current without any magnetic field has opened an alternate perspective for mass storage devices such as the Race Track Memory concept [1–3]. In this context, the use of materials with perpendicular magnetic anisotropy (PMA) is actively pursued [4]. The large anisotropy values in these materials lead to narrow DWs (typically about 1–20 nm) making them good candidates for extending the scaling of spintronics devices down to the nanometer scale. Narrow DWs interact very strongly with nanoscale inhomogeneities present in thin magnetic films, giving rise to random pinning events. Such a pinning effect introduces stochastic DW dynamics from one side involving thermal activation over the energy barrier at zero applied [5] force and on the other side deformation of the DW profile leading to a collective creep process [6–8]. One crucial issue for the Race Track Memory concept is to efficiently and reproducibly store multiple DWs at periodic positions along the wires. In order to achieve this, one possible way is to use lithographically defined constrictions along the nanowires [1]. In particular,

a reduction of the wire width at specified locations induces a potential well for the DW since it has to increase its length to propagate further, a process that generates an increase of DW energy [9]. This approach has been used efficiently for in-plane and out-of-plane materials, but it suffers from several drawbacks. First, the development of a high density of constrictions along a nanoscale wire, which exhibit the same properties, is a considerable nanotechnology challenge. Second, sharp constrictions such as, for instance, notches, can strongly affect the profile of the DW. Alternative methods based on local variations of magnetic anisotropy using ion irradiation [10,11] or exchange bias [12] have also been proposed, although these are not fully compatible with nanoscale dimensions and large-scale mass production. An elegant approach is based on nanoscale step edges that can be induced by a well-controlled epitaxial growth process [13,14]. In this case, very anisotropic DWs propagation and strong pinning at edges' steps have been reported due to the local variation of anisotropy and exchange stiffness. However, a crucial issue is related to the control of the steps' density and height on a large scale. Also, only ultra-thin magnetic films (1–2 monolayers) grown epitaxially on crystals can exhibit atomic step edges, which limits the range of usable materials and substrates. Finally, a recent study [15] has shown that locally etching the magnetic layer can also induce

\*roberto.mantovan@mdm.imm.cnr.it

†dafine.ravelosona@C2N.upsaclay.fr

local DW pinning. However, this approach involved an ion beam etching process, which introduces uncontrolled patterning-induced damage.

Our approach makes use of prepatterned substrates where regularly spaced nanoscale steps are created. This approach has already been used successfully for bit-patterned media [16,17] and has been shown to be an efficient route for manipulating the dynamics of spin waves in magnonic devices [18–20]. Successful growth of high structural quality Ta/Co-Fe-B(1 nm)/MgO(2 nm) ultra-thin films characterized by PMA is obtained on the modulated surface. These materials are considered the most promising not only for Spin Transfer Torque or Spin-Orbit Torque magnetic random-access memory (STT MRAM and SOT MRAM) [19], but also for Race Track memory devices [4,5,22–24] since they exhibit a high tunneling magneto-resistance ratio. We demonstrate that the subnanometer steps act as efficient sites for DW pinning when the DWs move across the steps and as a very efficient conduct when they move along the steps. Our results constitute a proof-of-concept for the possibility to manipulate the magnetic properties (anisotropy, DW dynamics, etc.) of ultra-thin films (1 nm) by employing subnanometer patterning. This could readily impact the technology transfer of nanoscaled emerging device concepts over large areas since the process flow is fully compatible with standard microelectronics manufacturing capabilities.

## II. SUBSTRATE PREPATTERNING PROCESS AND GROWTH OF Ta/Co-Fe-B/MgO STACKS

Eight inches (8") SiO<sub>2</sub> wafers are treated in order to create a surface modulation made of parallel subnanometer Si<sub>3</sub>N<sub>4</sub> steps with a period of 100 nm. Regular sinusoidal-like steps with a very low distribution of height and separation distance are obtained by using a combination of advanced nanotechnology CMOS processes involving selective etching processes of SiO<sub>2</sub> and Si<sub>3</sub>N<sub>4</sub> materials, nanolithography, and chemical mechanical polishing (Supplementary Information S1 [25]). This process is compatible with large-scale mass production, which is already being employed in the microelectronics industry. We use a pattern pitch of 100 nm, with a lateral width for trenches and steps of about 70 and 30 nm, respectively. Two different step heights (h) have been realized, as measured by AFM: high steps (HS) with h = 0.76(3) nm, and low steps (LS) with h = 0.25(4) nm (see Supplementary Information S1 [25]).

Following the realization of the prepatterned substrates, Ta(*t*<sub>Ta</sub>)/Co<sub>40</sub>Fe<sub>40</sub>B<sub>20</sub>(1 nm)/MgO(2 nm)/Ta(5 nm) stacks are deposited at room temperature by magnetron sputtering using a TIMARIS Singulus tool [5,19–21]. In order to optimize the magnetic properties, two distinct thicknesses of the bottom Ta layer are adopted: *t*<sub>Ta</sub> = 2 or 5 nm. Following stack deposition, in the case of *t*<sub>Ta</sub> = 2 nm, the average step

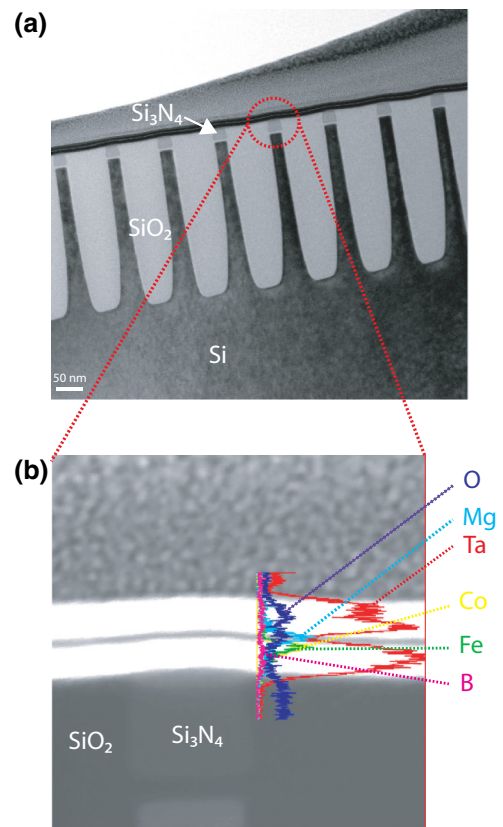


FIG. 1. (a) Cross-section TEM of the stack with  $t_{\text{Ta}} = 5$  nm on top of the HS substrate. (b) Magnification at the edge of a single step also showing the electron image profile from which the different layers in the stack are well identified.

height at the surface, as measured by AFM, is 0.58(8) nm and 0.11(6) nm for the HS and LS substrates, respectively. Cross-section TEM indicates that the different layers in the stack are well identified and follow the profile of the substrate underneath [see Fig. 1(a) for the case of  $t_{\text{Ta}} = 5$  nm on top of the HS substrate]. Figure 1(b) shows a magnification at the edge of a single step, where the electron image profile clearly shows that the different layers in the stack are well identified.

## III. RESULTS AND DISCUSSION

### A. Magnetic properties of the Ta/Co-Fe-B/MgO stacks

Following deposition in the amorphous state, the films are crystallized by a post-thermal annealing treatment at 300 °C for 2 h. As evidenced by hysteresis curves measured by polar magneto-optical kerr effect (P-MOKE) for amorphous and crystalline stacks (Supplementary Information S2 [25]) with  $t_{\text{Ta}} = 2$  nm grown on top of the LS and HS substrates, all the samples display PMA in both crystalline and amorphous cases, as previously observed for the same Co-Fe-B composition deposited

TABLE I. Values of coercive fields  $H_C$  and anisotropy constant  $H_{K\text{eff}}$  for the full set of samples discussed in the text.

Prepatterning	$t_{\text{Ta}}$ (nm)	stack	$H_C$ (mT)	$H_{K\text{eff}}$ (mT)
HS (0.76 nm)	2	Amorphous	2.2 (2)	50 (15)
HS (0.76 nm)	2	Crystalline	2.5 (1)	370 (40)
LS (0.25 nm)	2	Amorphous	2.0 (2)	120 (20)
LS (0.25 nm)	2	Crystalline	2.7 (1)	430 (40)
HS (0.76 nm)	5	Crystalline	1.9 (2)	390 (40)
LS (0.25 nm)	5	Crystalline	1.3 (2)	410 (40)

on top of flat Si/SiO<sub>2</sub> substrates [5,22]. On the other hand, for  $t_{\text{Ta}} = 5$  nm, PMA develops only following thermal annealing. Table I shows the magnetic parameters of the films, including the coercivity field  $H_C$  and the effective anisotropy field  $H_{K\text{eff}}$  determined by vector network analyzer ferromagnetic resonance (VNA-FMR) measurements [26–28] defined as  $H_{K\text{eff}} = 2K_{\text{eff}}/(\mu_0 M_S)$ , where  $K_{\text{eff}} = K_s/t - (1/2)(\mu_0 M_S^2)$  is the effective magnetic anisotropy with  $K_s$  the interface anisotropy and  $M_S$  the saturation magnetization. The coercivity here of around 2 mT for all the samples slightly increases with annealing as previously observed for films deposited on flat substrates, as a consequence of an increase of PMA in the crystalline state [21]. Different step heights do not seem to substantially alter  $H_C$  in both amorphous and crystalline samples. It can be noted that  $H_C$  values are slightly larger than those measured for similar stacks (same Co-Fe-B composition) grown on top of flat substrates, where  $H_C$  of 0.8 and 1.2 mT have been obtained for amorphous and crystalline states, respectively [22–24]. As indicated by Polar Kerr microscopy, the coercivity field  $H_C$  corresponds to the nucleation of a reversed domain on weak extrinsic sites, which may be different on prepatterned substrates that have been treated by successive nanofabrication processes. The values of  $H_{K\text{eff}}$  are also close to those obtained for similar stacks on top of flat substrates [22–24]. In particular, thermal treatment is efficient in increasing the anisotropy strength due to the crystallization of the Co-Fe-B layer. Note that the measured effective anisotropy field  $H_{K\text{eff}}$  indicated in Table I represents an average value over the patterned area, which includes a local variation of magnetic anisotropy due to the presence of steps (30% of the total surface). In particular, we observe that the values of  $H_{K\text{eff}}$  are lower for HS substrates, which indicates that large-step amplitudes influence PMA properties more strongly in ultra-thin Co-Fe-B layers, possibly by modifying the Ta/Co-Fe-B and/or Co-Fe-B/MgO interface anisotropy more efficiently. This strongly influences DW motion as discussed below.

### B. Domain-wall motion in ultrathin Co-Fe-B-based systems on prepatterned substrates

Figure 2(a) displays the configuration of the experiment for the DWs velocity measurement in Ta( $t_{\text{Ta}}$ )/Co<sub>40</sub>Fe<sub>40</sub>B<sub>20</sub>

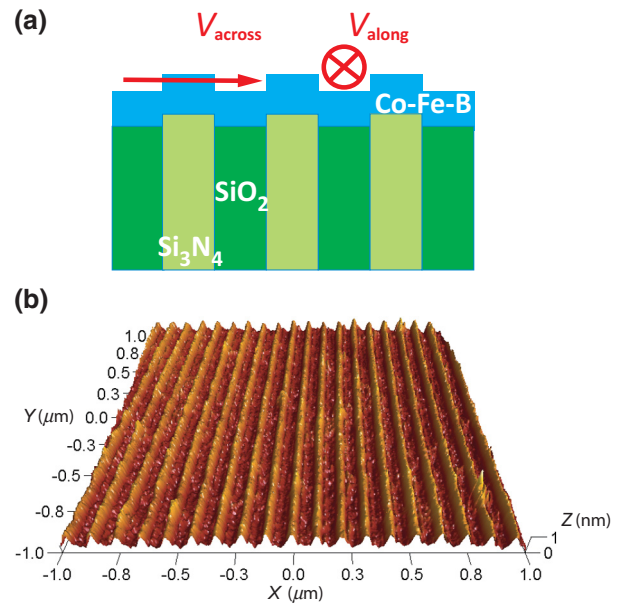


FIG. 2. (a) Schematic of the experiment of DW motion in Ta( $t_{\text{Ta}}$ )/Co<sub>40</sub>Fe<sub>40</sub>B<sub>20</sub>(1 nm)/MgO(2 nm)/Ta(5 nm) ultra-thin films grown on top of prepatterned substrates; The pattern pitch is 100 nm and the lateral widths of the trenches (SiO<sub>2</sub>) and steps (Si<sub>3</sub>N<sub>4</sub>) are 70 and 30 nm, respectively. (b) AFM of the stack with  $t_{\text{Ta}} = 2$  nm, deposited on top of the HS substrate: following stack deposition, the average step height at the surface is 0.58(8) nm.

(1 nm)/MgO(2 nm)/Ta(5 nm) on top of prepatterned substrates, with  $V_{\text{across}}$  and  $V_{\text{along}}$  the velocities across and along the stripes, respectively. Figure 2(b) shows the AFM of the stack with  $t_{\text{Ta}} = 2$  nm on top of the HS substrate, where the DW experiments are conducted.

Figures 3(a) and 3(b) show Kerr microscopy images of the DWs' motion measured in the amorphous stacks with  $t_{\text{Ta}} = 2$  nm, indicating DWs moving along and across the steps on top of the HS substrate. Figure 3(a) corresponds to the image before the application of a magnetic pulse, whereas Fig. 3(b) is the image difference before and after applying the magnetic field pulse. It can be clearly observed that DW propagation is highly anisotropic, being favored (impeded) along (across) the steps, respectively. In particular, as seen in Fig. 3(b) after the application of a magnetic field pulse, the DW moves faster along the steps (L2) than across them (L1). Also, it can be noted that the DW velocity is roughly the same for the nonpatterned area (L3) and along the steps (L2). For annealed films, it has not been possible to observe DWs motion across the steps, but only along the “valleys.” This is an indication that the energy barrier for DW motion across the steps is largely increased during crystallization, making the steps act as extremely strong pinning sites. The results in Fig. 3 clearly demonstrate that prepatterned subnanometer steps strongly influence DWs dynamics by inducing anisotropic motion.



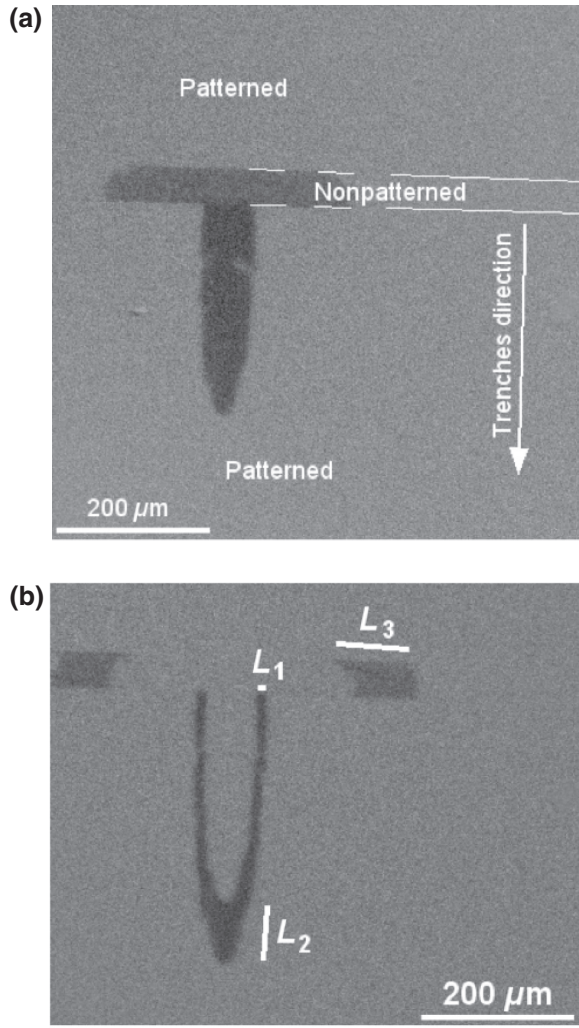


FIG. 3. Kerr Microscopy imaging of DWs moving from a nonpatterned to a patterned area in an amorphous Ta(2 nm)/Co-Fe-B(1 nm)/MgO(2 nm)/Ta(5 nm) stack on top of the HS substrate. (a) Image before the application of a magnetic pulse. (b) Image difference before and after applying a magnetic field pulse.

Figures 4(a) and 4(b) report the DW velocities in the stacks with  $t_{\text{Ta}}=2$  nm on top of LS and HS substrates. Consistent with the Kerr images of Fig. 3, a strong reduction of DW velocity is observed for the amorphous case when the DW propagates across the steps for both LS and HS substrates. For instance, on top of the LS (amorphous case), at 1 mT, velocities along and across the steps are, respectively,  $V_{\text{along}}(\text{amorphous})\sim 14800 \mu\text{m/s}$  and  $V_{\text{across}}(\text{amorphous})\sim 1500 \mu\text{m/s}$ , which correspond to a ratio of  $V_{\text{along}}/V_{\text{across}}\sim 10$ . On top of the HS substrate (amorphous case), velocities at 1 mT are  $V_{\text{along}}(\text{amorphous})\sim 3000 \mu\text{m/s}$  and  $V_{\text{across}}(\text{amorphous})\sim 40 \mu\text{m/s}$ , i.e., a ratio of  $V_{\text{along}}/V_{\text{across}}\sim 70$  is obtained. In addition, we observe that the DW velocity is always lower for HS than LS substrates indicating that higher steps are

more efficient in pinning DWs. Finally, we note that  $V_{\text{along}}(\text{crystalline})$  is always lower than  $V_{\text{along}}(\text{amorphous})$  for both HS and LS substrates. At 1 mT for instance, we show ratios  $V_{\text{along}}(\text{amorphous})/V_{\text{along}}(\text{crystalline})$  of 170 and 370 on top of LS and HS, respectively.

As indicated in Figs. 4(c) and 4(d), the DW velocity follows a creep behavior [6–8] with  $v = v_0 \exp[-(U_C/k_B T)(H_P/H)^{1/4}]$ , where  $v_0$  is a characteristic velocity,  $U_C$  is a characteristic energy,  $k_B$  is the Boltzmann constant,  $T$  is the temperature, and  $H_P$  is the depinning field at zero temperature. This thermally activated regime describes the collective pinning of the DW by structural defects present in the film. As for Co-Fe-B ultra-thin films deposited on flat substrates, the exponent 1/4 fits the data well and is theoretically predicted for the interaction of a one-dimensional DW with two-dimensional weak random disorder [29]. The fact that the creep law is still valid in the presence of a periodic potential is consistent with our previous study demonstrating that only the depinning field is renormalized whereas the universality class does not change [30]. Figure 5 summarizes the  $H_P$  values derived from the fit of the curves in Fig. 4 in the case of  $t_{\text{Ta}}=2$  nm on top of both LS and HS substrates. Taking  $U_C/k_B T\sim 20$  from the value reported for a similar material stack on top of flat Si/SiO<sub>2</sub> substrates [8,22], we find for the amorphous sample  $H_{P\text{across}}(\text{LS})=2$  mT and  $H_{P\text{across}}(\text{HS})=9$  mT in the case of motion across the steps, which corresponds to an almost 2–4 times larger field than those obtained along the steps [ $H_{P\text{along}}(\text{LS})=1$  mT and  $H_{P\text{along}}(\text{HS})=2$  mT], confirming the efficient storing pinning schemes. These values also confirm that the HS substrates are more efficient in preventing the DWs from propagating across the steps.

The increase of the DW pinning strength across the steps can originate from the local variation of magnetic anisotropy between the trenches and the steps. Particularly, the anisotropy can be either slightly tilted or reduced in strength across the steps, inducing a potential well for the DW. More precisely, the presence of a gradient of perpendicular anisotropy on a length scale  $\delta$  leads to a local pinning field given by [11,31]:

$$H_{P\text{across}} = (H_{K\text{trench}} - H_{K\text{step}}) \cdot \frac{2\Delta}{\delta} \tanh\left(\frac{\delta}{2\Delta}\right), \quad (1)$$

where  $H_{K\text{trench}}$  and  $H_{K\text{step}}$  are the effective anisotropy field for the trenches and the steps, respectively, and  $\Delta$  is the DW width. By using an anisotropy gradient length of  $\delta\sim\Delta$  corresponding approximately to the step width, and considering that  $H_{K\text{trench}}$  can be approximated by the average value  $H_{K\text{eff}}$  as measured in Table I, Eq. (1) gives for the amorphous sample  $H_{K\text{step}}(\text{LS})\sim 120$  mT and  $H_{K\text{step}}(\text{HS})\sim 40$  mT. This corresponds to a local reduction of anisotropy induced by the steps of about 1% and 20% for LS and HS substrates, respectively (Table I). In the

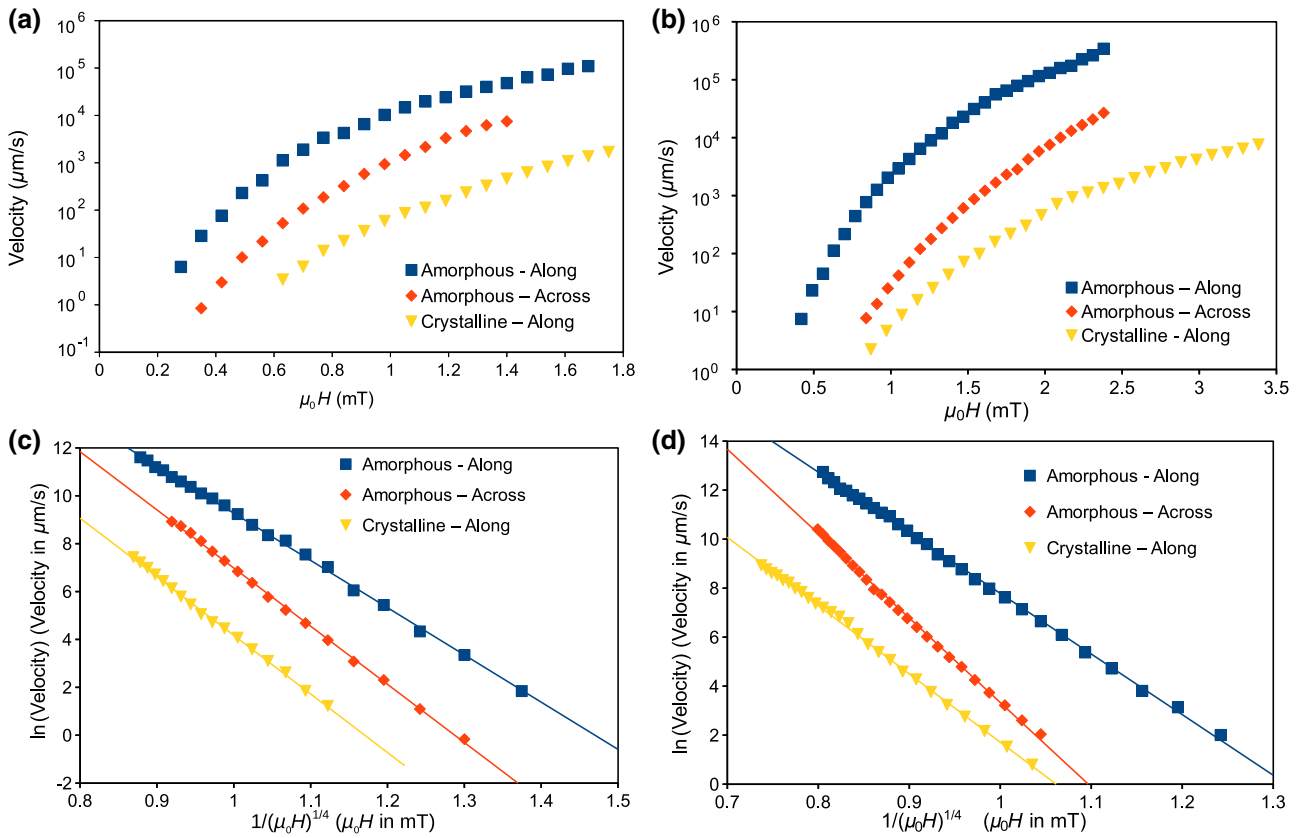


FIG. 4. DW velocities at different applied magnetic fields for amorphous and crystalline stacks on top of LS (a) and HS (b) substrates, respectively. Corresponding velocity (in logarithmic scale) as a function of  $H^{-1/4}$  for amorphous and crystalline stacks on top of LS (c) and HS (d) substrates, respectively.

case of motion along the steps in annealed (crystalline) samples, there is an enhancement by a factor of 2 of the depinning field as compared to the motion along the steps in the amorphous case. The increase in pinning strength in the annealed samples arises first from the higher anisotropy

value obtained in the crystalline state, but also from the additional structural disorder induced by the annealing process at high temperatures as shown previously in Co-Fe-B-based structures grown on top of flat substrates [22–24]. The crystallization process on prepatterned substrates may be affected by the topology, especially for the HS substrates, which indicates that further optimization of the annealing process is needed.

Finally, a striking result is that the propagation fields along the 70 nm conducts for both amorphous and crystalline structures on LS and HS substrates are one order of magnitude lower than those reported on larger-patterned nanowires [32,33], where edge damages, such as edge roughness induced by the patterning process, strongly affect the DW dynamics. Such easy DW motion along the narrow conduct is consistent with Fig. 3(b), where DW velocity along the trenches (see L2) is comparable to the DW velocity in the nonpatterned area (see L3). In addition, we note that the DW velocities along the steps for the HS case are lower than those for the LS case. When propagating along the steps, a fraction of the DW is sensitive to the steps where the anisotropy is reduced. In particular, when the anisotropy is reduced by 20% in the HS case, DW motion is expected to be more affected.

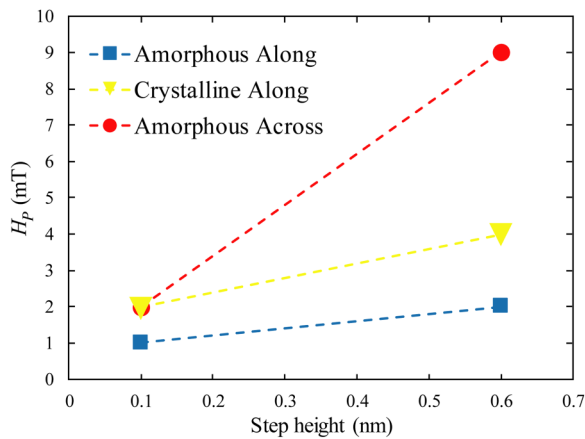


FIG. 5. Depinning fields for amorphous and crystalline stacks on top of LS and HS substrates.

#### IV. CONCLUSION

The manipulation of magnetic DWs in magnetic nanowires provides an exciting opportunity to develop additional concepts for ultra-high-density spintronic devices. In this work, we have shown the possibility to develop efficient DW pinning in Co-Fe-B/MgO ultra-thin films displaying PMA, by engineering subnanometer steps at the surface of the substrate. Our method is adopted from a well-known CMOS industrial process, therefore, it is compatible with low-cost and large-scale mass production. By making use of double patterning, steps could be quite easily generated with a pitch scalable to the limits of lithography of less than 10 nm, thus providing a viable way to target an “ultimate” scalability of the Race Track memory concept by making use of artificial prepatterned pinning sites and nanowires perpendicular to the steps. Finally, the possibility to channel DW motion along the steps may be a promising solution to overcome the crucial issue related to edge damages at very small wire dimensions [24,32–34].

#### ACKNOWLEDGMENTS

This work was supported by the European Union FP7 program through Contract MAGWIRE Grant No. 257707 and the ANR-NSF COMAG project.

- 
- [1] S. S. P. Parkin, M. Hayashi, and L. Thomas, Magnetic domain-wall racetrack memory, *Science* **320**, 190 (2008).
  - [2] Claude Chappert, Albert Fert, and Frédéric Nguyen Van Dau, The emergence of spin electronics in data storage, *Nat. Mater.* **6**, 813 (2007).
  - [3] A. Brataas, A. D. Kent, and H. Ohno, Current induced torque in magnetic materials, *Nat. Mater.* **11**, 372 (2012).
  - [4] Y. Zhang, W. S. Zhao, D. Ravelosona, J.-O. Klein, J. V. Kim, and C. Chappert, Perpendicular magnetic anisotropy CoFeB racetrack memory, *J. Appl. Phys.* **111**, 093925 (2012).
  - [5] J.-P. Tetienne, T. Hingant, J.-V. Kim, L. Herrera Diez, J.-P. Adam, K. Garcia, J.-F. Roch, S. Rohart, A. Thiaville, D. Ravelosona, and V. Jacques, Nanoscale imaging and control of domain-wall hopping with a nitrogen-vacancy center microscope, *Science* **344**, 1366 (2014).
  - [6] P. J. Metaxas, J. P. Jamet, A. Mougin, M. Cormier, J. Ferré, V. Baltz, B. Rodmacq, B. Dieny, and R. L. Stamps, Creep and Flow Regimes of Magnetic Domain-Wall Motion in Ultrathin Pt/Co/Pt Films with Perpendicular Anisotropy, *Phys. Rev. Lett.* **99**, 217208 (2007).
  - [7] J. Ferré, Dynamics of Magnetization Reversal: From Continuous to Patterned Ferromagnetic Films, in *Spin Dynamics in Confined Magnetic Structures I*, edited by B. Hillebrands and K. Ounadjela (Springer-Verlag Berlin Heidelberg, 2002), Vol. 83, p. 127.
  - [8] D. Ravelosona, Dynamics of Domain Wall Motion in Wires with Perpendicular Anisotropy, in *Nanoscale Materials and Applications* (Springer-Verlag, New York, 2009).
  - [9] J. Wunderlich, D. Ravelosona, C. Chappert, F. Cayssol, V. Mathet, J. Ferre, J. P. Jamet, and A. Thiaville, Influence of geometry on domain wall propagation in a mesoscopic wire, *IEEE Trans. Magn.* **37**, 2104 (2001).
  - [10] C. Chappert, H. Bernas, J. Ferré, V. Kottle, J. P. Jamet, Y. Chen, E. Cambril, T. Devolder, F. Rousseaux, V. Mathet, and H. Launois, Planar patterned magnetic media obtained by ion irradiation, *Science* **280**, 1919 (1998).
  - [11] J. H. Franken, M. Hoeijmakers, R. Lavrijsen, and H. J. M. Swagten, Domain-wall pinning by local control of anisotropy in Pt/Co/Pt strips, *J. Phys.: Condens. Matter* **24**, 024216 (2012).
  - [12] I. Polenciuc, A. J. Vick, D. Allwood, T. J. Hayward, G. Vallejo-Fernandez, K. O’Grady, and A. Hirohata, Domain wall pinning for racetrack memory using exchange bias, *Appl. Phys. Lett.* **105**, 162406 (2014).
  - [13] P. Haibach, M. Huth, and H. Adrian, Step edge induced anisotropic domain wall propagation, *Phys. Rev. Lett.* **84**, 1312 (2000).
  - [14] S. Bodea, W. Wulfhekel, and J. Kirschner, Influence of step edges and strain on the domain wall width, *Phys. Rev. B* **72**, 100403 (2005).
  - [15] T. Hironobu, K. Kondou, T. Koyama, K. Nakano, S. Kasai, N. Ohshima, S. Fukami, N. shiwata, and T. Ono, Current-driven domain wall motion in CoCrPt wires with perpendicular magnetic anisotropy, *Appl. Phys. Exp.* **1**, 011301 (2008).
  - [16] T. Thomson, G. Hu, and B. D. Terris, Intrinsic Distribution of Magnetic Anisotropy in Thin Films Probed by Patterned Nanostructures, *Phys. Rev. Lett.* **96**, 257204 (2006).
  - [17] O. Hellwig, A. Moser, E. Dobisz, Z. Z. Bandic, H. Yang, D. S. Kercher, J. D. Risner- Jamtgaard, D. Yaney, and E. E. Fullerton, Coercivity tuning in Co/Pd multilayer based bit patterned media, *Appl. Phys. Lett.* **93**, 192501 (2008).
  - [18] V. E. Demidov, S. Urazhdin, A. Zhulud, A. V. Sadovnikov, and S. O. Demokritov, Dipolar field-induced spin-wave waveguides for spin-torque magnonics, *Appl. Phys. Lett.* **106**, 022403 (2015).
  - [19] A. V. Sadovnikov, S. A. Odintsov, E. N. Beginin, S. E. Sheshukova, Yu. P. Sharaevskii, and S. A. Nikitov, Toward nonlinear magnonics: Intensity-dependent spin-wave switching in insulating side-coupled magnetic stripes, *Phys. Rev. B* **96**, 144428 (2017).
  - [20] A. V. Sadovnikov, A. A. Grachev, E. N. Beginin, S. E. Sheshukova, Yu. P. Sharaevskii, and S. A. Nikitov, Voltage-Controlled Spin-Wave Coupling in Adjacent Ferromagnetic-Ferroelectric Heterostructures, *Phys. Rev. Appl.* **7**, 014013 (2017).
  - [21] S. Ikeda, K. Miura, H. Yamamoto, K. Mizunuma, H. D. Gan, M. Endo, S. Kanai, J. Hayakawa, F. Matsukura, and H. Ohno, A perpendicular-anisotropy CoFeB–MgO magnetic tunnel junction, *Nat. Mater.* **9**, 721 (2010).
  - [22] C. Burrowes, N. Vernier, J.-P. Adam, L. Herrera Diez, K. Garcia, I. Barisic, G. Agnus, J.-V. Kim, T. Devolder, A. Lamperti, R. Mantovan, B. Ockert, E. Fullerton, and D. Ravelosona, Low depinning fields in Ta-CoFeB-MgO ultra-thin films with perpendicular magnetic anisotropy, *Appl. Phys. Lett.* **103**, 182401 (2013).
  - [23] R. Mantovan, A. Lamperti, G. Tallarida, L. Baldi, M. Mariani, B. Ocker, S.-M. Ahn, I. Barisic, and D. Ravelosona, Perpendicular magnetic anisotropy in Ta/CoFeB/MgO

- systems synthesized on treated SiN/SiO<sub>2</sub> substrates for magnetic memories, *Thin Solid Films* **533**, 75 (2013).
- [24] A. Lamperti, S.-M. Ahn, B. Ocker, R. Mantovan, and D. Ravelosona, Interface width evaluation in thin layered CoFeB/MgO multilayers including Ru or Ta buffer layer by X-ray reflectivity, *Thin Solid Films* **533**, 79 (2013).
- [25] See supplementary materials at <http://link.aps.org/supplemental/10.1103/PhysRevApplied.10.064053> for the fabrication of pre-patterned substrates and the magnetic characterizations of the CoFeB-MgO stacks
- [26] C. Bilzer, T. Devolder, P. Crozat, and C. Chappert, Open-circuit one-port network analyzer ferromagnetic resonance, *IEEE Trans. Magn.* **44**, 3265 (2008).
- [27] T. Devolder, P.-H. Ducrot, J.-P. Adam, I. Barisic, N. Vernier, J.-V. Kim, B. Ockert, and D. Ravelosona, Damping of Co<sub>x</sub>Fe<sub>80-x</sub>B<sub>20</sub> ultrathin films with perpendicular magnetic anisotropy, Irradiation-induced tailoring of the magnetism of CoFeB/MgO ultrathin films, *Appl. Phys. Lett.* **102**, 022407 (2013).
- [28] T. Devolder, I. Barisic, S. Eimer, K. Garcia, J.-P. Adam, B. Ockert, and D. Ravelosona, Irradiation-induced tailoring of the magnetism of CoFeB/MgO ultrathin films, *J. Appl. Phys.* **113**, 203912 (2013).
- [29] S. Lemerle, J. Ferré, C. Chappert, V. Mathet, T. Giamarchi, and P. Le Doussal, Domain Wall Creep in an Ising Ultrathin Magnetic Film, *Phys. Rev. Lett.* **80**, 849 (1998).
- [30] F. Cayssol, D. Ravelosona, C. Chappert, J. Ferré, and J. P. Jamet, Domain Wall Creep in Magnetic Wires, *Phys. Rev. Lett.* **92**, 107202 (2004).
- [31] J. H. Franken, M. Hoeijmakers, R. Lavrijsen, J. T. Kohlhepp, H. J. M. Swagten, B. Koopmans, E. Van Veldhoven, and D. J. Maas, Precise control of domain wall injection and pinning using helium and gallium focused ion beams, *J. Appl. Phys.* **109**, 07D504 (2011).
- [32] X. Zhang, N. Vernier, W. Zhao, L. Vila, and D. Ravelosona, Extrinsic pinning of magnetic domain walls in CoFeB-MgO nanowires with perpendicular anisotropy, *AIP Adv.* **8**, 056307 (2018).
- [33] L. Herrera Diez, V. Jeudy, G. Durin, A. Casiraghi, Y. T. Liu, M. Voto, G. Agnus, D. Bouville, L. Vila, J. Langer, B. Ocker, L. Lopez-Diaz, and D. Ravelosona, Wire edge dependent magnetic domain wall creep, *Phys. Rev B* **98**, 054417 (2018).
- [34] J. P. Jamet, J. Ferré, P. Meyer, J. Gierak, C. Vieu, F. Rousseaux, C. Chappert, and V. Mathet, Giant enhancement of the domain wall velocity in irradiated ultrathin magnetic nanowires, *IEEE Trans. Magn.* **37**, 4 (2001).